EXPERIMENT REPORT

Ricardo José Chimenton

ESRF	Experiment title: **In situ powder diffraction of the formation of metal carbides confined in the porous channels of SBA-15. A potential novel catalytic material for biomass hydrogenolysis.**	**Experiment number**: MA1525
Beamline: BM25A	**Date of experiment**: from: 07/11/2012 at 08:00 to: 12/11/2012 at 08:00	**Date of report**:
Shifts: 15	**Local contact(s): Alvaro Muñoz Noval** **alvaro.muñoz-noval@esrf.fr**	*Received at ESRF:*

Names and affiliations of applicants (* indicates experimentalists):

Dr. Ricardo CHIMENTON (ricardojose.chimenton@urv.cat)[1,*]

Edgar JIMENEZ GUELL (edgarbiotec8@gmail.com)[1,*]

Dr. Luis B. MODESTO-LOPEZ (luis.modesto@urv.cat)[1,*]

Dr. Joan ROSELL-LLOMPART (joan.rosell@urv.cat)[1,2,*]

[1]**Chemical Engineering Department, University Rovira i Virgili, Tarragona (Spain)**

[2]**Catalan Institution for Research and Advanced Studies (ICREA), Barcelona (Spain)**

Scope of the experiment

The aim of the measurements was the characterization by *in situ* X-ray powder synchrotron diffraction of the carburization of Mo and W confined in the channels of mesoporous silica (SBA-15) support, and on γ-Al_2O_3 and on Mg-Al-O. *In situ* X-ray analysis can provide detailed information about the formation of the metal carbide during temperature programmed carburization (TPC) process. During the experiment we decided to also include measurements of the reduction of nickel nitrate impregnated over gamma alumina in order to verify the consistency of the setup.

1. Objective

The main objective was to study the evolution of the carbide formation and stability of the mesoporous support by XRD *in situ* analysis during the temperature program from d spacings of ~99Å up to 1.6 Å.

2. Experimental

The powder samples in pellet form were mounted in a IR transmission cell provided by BM25A SpLine. This cell reactor was a HPHT (high pressure high termperature) cell from SPECAC Brillant Spectroscopy, which ESRF personnel had modified with kapton windows in order to reduce X-ray absorption. The gas flow lines and controller system, also provided by SpLine, were attached to the cell. Temperature programmed carburization (TPC) of the loaded samples was performed under flowing CH_4/H_2 (20/80 v/v) gas mixture. For the *in situ* study of the metal carbide formation, the temperature was ramped linearly from room temperature at either of two rates, 2.5 or 5 °C/min. During the cooling stage, the CH_4/H_2 mixed gas was switched to argon.

Approximately 100 mg of dried sample was placed in a metallic sample holder, and were then hand pressed into a thin pellet (1.0 cm diameter and 0.25 cm thickness). The pellet sample was then placed in the cell reactor to be analyzed in transmission mode (2x2 mm^2 aproximate beam size). The diffracted X-rays were recorded on an beam-axis-motorized CCD detector (charge-coupled device) placed 34 cm away from the sample. The X-ray wavelength used was 0.6199 Å (20 keV) and the Bragg angle was scanned continuously in the range $2\theta = 2.2°– 22°$. The exposure time for the CCD detector was 300 s typically. The CCD images (ca. 68 scans) were acquired *in situ* while the sample was heated in a H_2/methane stream. Prior to each analysis, the CCD was calibrated by analyzing α-Al_2O_3 (SRM 676) prepared in the same conditions.

Each CCD image was converted to conventional 2θ-diffractograms by azimuthal integration (X-ray Oriented Programs, XOP 2.3 Software). Subsequent treatment for quantification of the crystalline phases was performed by the Rietveld method at Universitat Rovira i Virgili, by using the software TOPAS 4.2.

2. Samples

The XRD measurements were performed on the following samples:

(i) α-Al_2O_3 (corundum SRM 676) (reference for CCD);
(ii) nickel nitrate impregnated over gamma-alumina (reference for reduction);
(iii) WO_3 supported on γ-Al_2O_3 and on Mg-Al-O (for carburization);
(iv) WO_3 supported on SBA-15 and SBA-15 (Si/Al= 10) (for carburization);
(v) MoO_3 supported on Al_2O_3 and Mg-Al-O (for carburization).

3. Results

A brief summary of the results obtained from the samples (i, ii) and (iv, v) is presented.

During the experimentation we quickly realized that under the carburization experiments, the cell temperature saturated at about 700ºC, before the carburization had been completed. As we tried to deal with this limitation, a reference for reduction was run in order to verify the correct operation of the reaction cell arrangement for a sample that would react at slightly lower temperatures. Fig. 1a shows the XRD patterns of this reference sample, namely $Ni(NO_3)_2 \cdot 6H_2O$ impregnated over γ-Al_2O_3 reduced *in situ* under flow of H_2. The evolution in the crystalline phases during the reduction process can be clearly observed. Two prominent reflections which could be assigned only to $(Ni(OH)_2(NiOOH)_{0.167})_{0.857}$ (**a**: 3.071 c: 23.200, R-3m, Jamborite, ICDD 89-7111, ICSD 76650) are evident in the diffractograms obtained as the dried sample was heated from RT to about 600 K. These two peaks correspond to the (003) and (006) planes of the Jamborite phase. It is important to mention that the

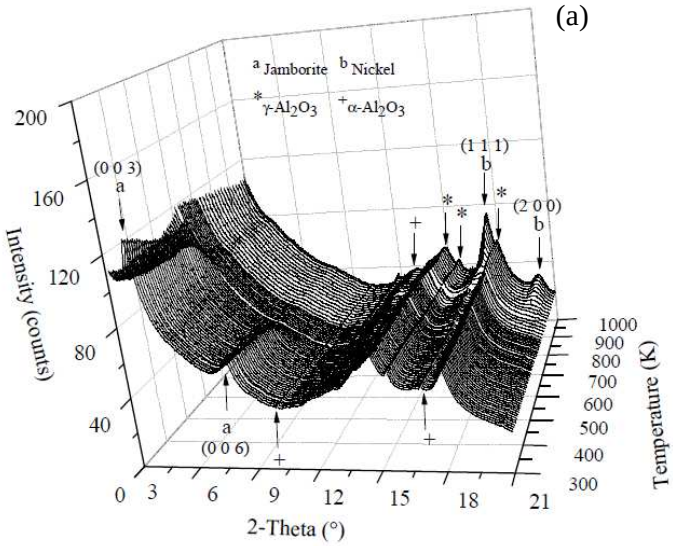

Figure 1. *In situ* XRD nickel nitrate precursor impregnated on γ-Al_2O_3.

peaks detected are far from the expected position for pure Jamborite. In our case, the **a** parameter at room T was ≈26.4Å whereas the theoretical value was 23.2 Å. This difference indicates that the stoichiometry of our phase is not exactly the same that published in the literature. This difference is possible due to the layered structure of Jamborite.

Thus, *in situ* XRD has showed that the decomposition of the Jamborite phase occurred between 400-600 K. The XRD patterns (Fig. 1a) also show peaks for metallic Ni above 800 K, corresponding to planes (111) and (200) (ICDD 4-0850).

Fig. 1b exhibits the Rietveld quantification of the crystalline phases during the *in situ* reduction of the nickel nitrate precursor. The Jamborite phase clearly decomposes at about 600 K and metallic Ni starts to appear at about 830 K. We took the resulting diffractogram of the corundum standard to derive the instrumental resolution function of our setup by three dependent convolutions. Previously, the corundum standard had been characterized in our lab with LaB6 (SRM 660a) in order to determine its mean crystallite size. The crystallite size of the different phases was estimated by the Double-Voigth approach and applying the modified Scherrer expression for the integral breadth.

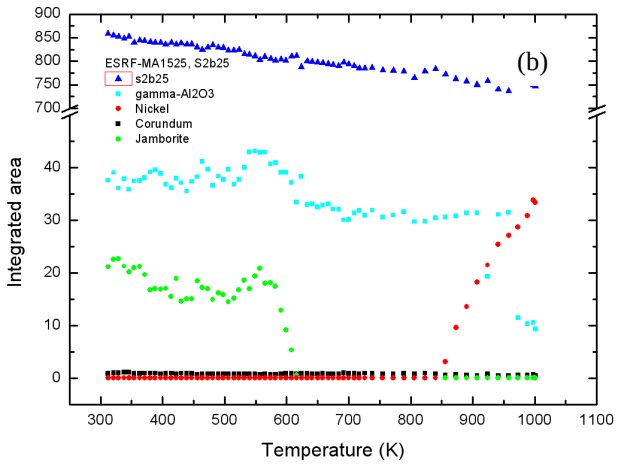

Figure 1. Evolution of the crystaline phases in the reduction of the nickel nitrate precursor impregnated on γ-Al_2O_3.

The structure of Jamborite (ICSD 76650) was not possible to use because our phase probably didn't have the same stoichiometry that the theoretical one, as we have mentioned before. So, we decided to use the area under the Jamborite peaks as an indicator of the phase diffracting mass. Fig. 1b shows how the integrated area for each phase involved changes as a funtion of T. In addition, the evolution of the background intensity (blue triangles) is shown to decrease with T, so indicating that a mass consumption (mainly not crystalline) is taking place during the annealing.

Fig. 2 expresses the evolution of the *in situ* temperature programmed carburization (TPC) process starting from monoclinic tungsten trioxide ($P2_1/n$) species supported on mesoporous silica SBA-15 and SBA-15 (Si/Al =10) supports. Fig. 2a and Fig. 2b illustrate the tungsten oxide phases in the caburization process of the monoclinic tungsten trioxide species supported over SBA-15 and SBA-

15 (Si/Al= 10) supports, respectively. The phases quantified by Rietveld method for the carburization of WO_3 ($P2_1/n$) supported supported over SBA-15 is shown in Fig 2c. Up to 600 K, the WO_3 ($P2_1/n$) species starts to decompose as a new phase appears, orthorhombic WO_3 (Pcnb) species. This species increases progressively in population until about 750 K and then drops progressively until the final stage of carburization is reached (at about 884 K). Other tungsten phases such as tetragonal WO_3 (P4ncc) and $W_{25}O_{73}$ (P2/C) starts to appear after about 700 K. The transition to tungsten carbides were incomplete in this case. Figs. 2d express the evolution the tungsten phases in the caburization process and the phases quantified by Rietveld method starting from monoclinic tungsten trioxide ($P2_1/n$) species supported on mesoporous silica SBA-15 (Si/Al=10). Carburization monoclinic tungsten trioxide ($P2_1/n$) species supported on mesoporous silica SBA-15 (Si/Al=10) shows the presence of more reduced state species of tungsten such as WO_2 ($P2_1/c$). The transition to tungsten carbide was not observed.

Fig. 3 shows the *in situ* XRD patterns and quantification of the phase during the temperature-programmed carburization process of the MoO_3 species supported over γ-Al_2O_3 and Mg-Al-O mixed oxide supports. Based on the Fig 3a and 3c the phases detected during the TPC programm of the MoO_3/γ-Al_2O_3 samples were: α-Al_2O_3 (JCPDS 46-1212), molybdite (MoO_3, JCPDS 005-0508), γ-Al_2O_3 (JCPDS 79-1558), and tugorinovite, MoO_2 (JCPDS 086-0135). And the phases identified during the carburization of the MoO_3 (Fig. 3b y 3d) supported on Mg-Al-O were: : Magnesium molybdenum oxide, $MgMoO_4$ (JCPDS 072-2153), molybedenum oxide, $Mo_{17}O_{47}$ (JCPDS 074-2265), periclase, MgO (JCPDS 045-0946), molyddenum oxide β-MoO_3 (JCPDS 089-1554), tugarinovite, MoO_2 (JCPDS 086-0135) and spinel $MgAl_2O_4$ (JCPDS 021-1152).

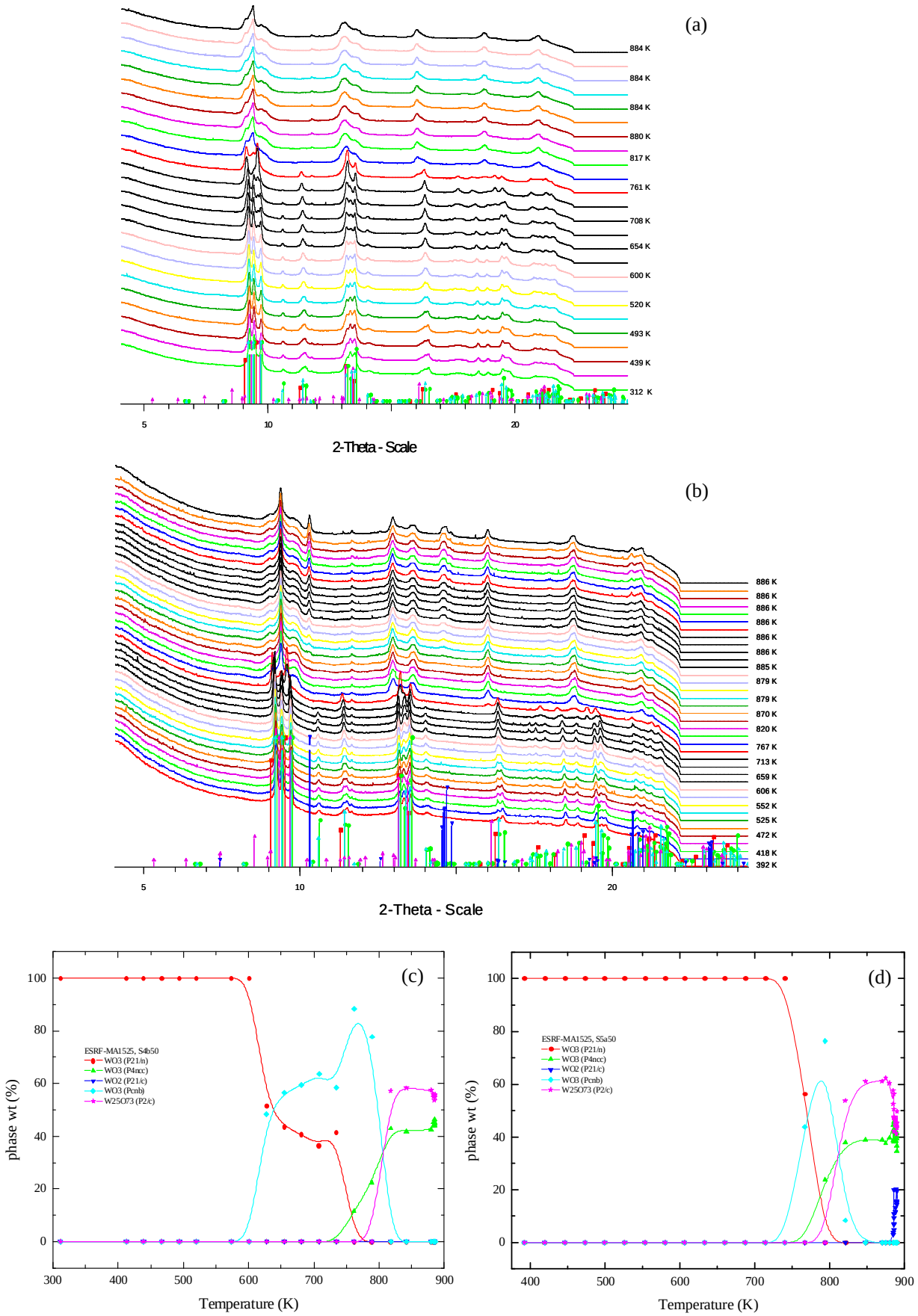

Fig 2. (a) *In situ* XRD patterns of the carburization process of the WO_3 species supported on (a) SBA-15 and on SBA-(b) 15 (Si/Al=10). Evolution of the crystallograffic phases during the carburization process of the WO_3 species supported on (c) SBA-15 and on (d) SBA-15 (Si/Al=10).

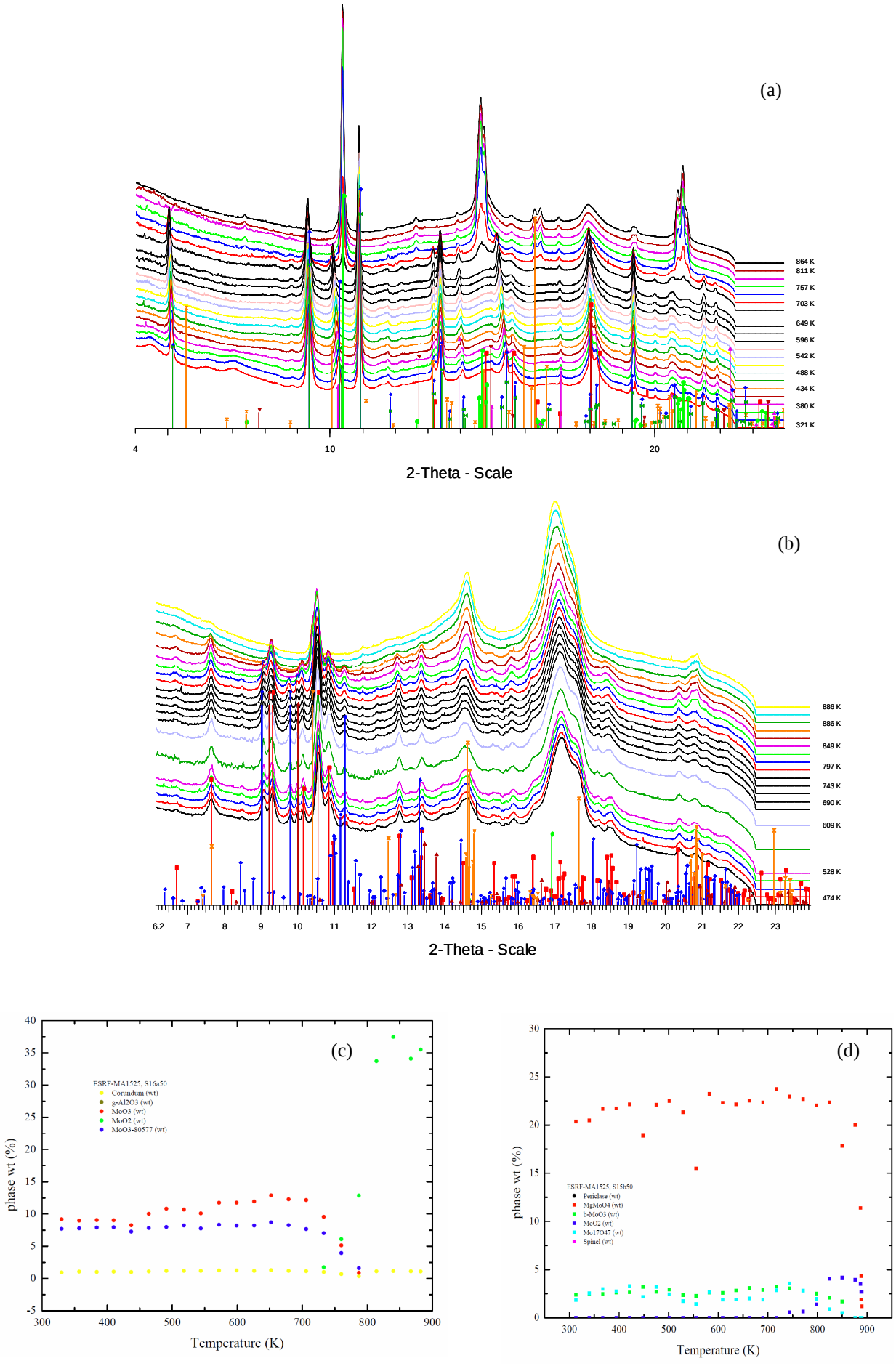

Fig 3. (a) *In situ* XRD patterns of the carburization process of the MoO_3 species supported on (a) γ-Al_2O_3 and (b) over Mg-Al-O mixed oxide. Evolution of the crystalline phases during the carburization process of the MoO_3 species on (c) over γ-Al_2O_3 and (d) on Mg-Al-O mixed oxide.

Observations

The present proposal was developed in the BM25A in the Spanish beam line in two stages; the first visit from June 21 till June 26, 2012, and the second one from November 7 till November 12, 2012. During our first visit, the XRD setup presented several problems which could not be overcome at that time. The CCD detector had been mounted in this line for the first time, and it was assembled on the line in such a way that both the sample-detector distance and its height had to be adjusted manually. We realised that with this detector it would be impossible to cover the desired d-space range. We decided to perform firstly the mean d-spacings and secondly try with high d-spacings. In addition, the setup did not have a proper beamstop, which had to be improvised with a piece of lead.

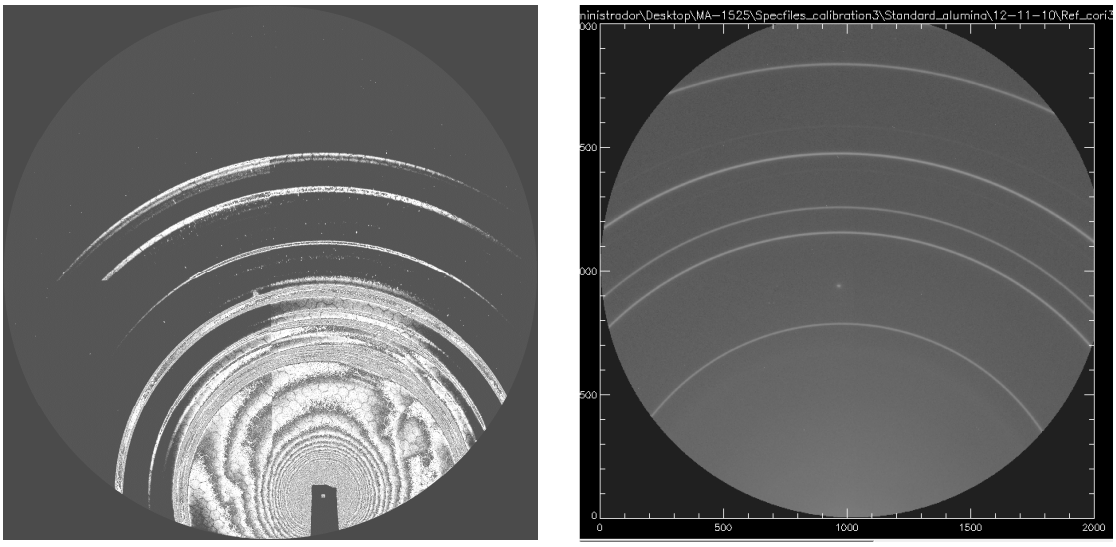

Fig 4. (a) CCD image of corundum standard in the first turn measurements (june-2012) and (b) CCD image of corundum standard in the second turn (november-2012).

In the first measurements of the corundum standard at room temperature, the CCD detector revealed a huge number of reflections of unknown origin and a quick decay of the intensity at high angles (Fig. 4a). So, the peaks detected were only the high intensity ones, but no peaks were detected for the lower intensity peaks. The resulting diffractogram with the CCD detector had poor resolution, unusuable for phase identification. In addition, the SPECAC cell presented a faulty electric contact.

In the second visit to ESRF, the set-up had been improved considerably. In this case the CCD camera presented 4 quadrants with well defined in sensitivity and, in general, all usable for integration. Occasionally one or two quadrants of the CCD camera presented different sensitivity compared to the others, with consequent reduction in signal to noise ratio, which had implications in the identification of some of the phases. But the XRD patterns had markedly increased signal to noise ratio with respect to the previous visit. This unstability of the CCD was translated into the

resulting diffractograms in a very changing and irregular background. As a result, the modellization of such background by the Rietveld method became too difficult in some cases, which ultimately had to be discarted in those calculations. Apart from that, most of the frames presented spurious spots (maybe due to cosmic radiation) that had to be delete manually (and painstakingly) before carrying out the integration of the frame.

On the other hand, the set up was also improved in terms of automatic operation, where both the beam stop and the CCD camera could be operated remotely from the control room. In addtion, the faulty electric contact in the SPECAC cell had been fixed. However, it was possible to heat up the cell to 700ºC easily, but not to the 800ºC that had been requested in the project proposal, except for some gas compositions at the small heating rate. As a result of this limitation, the total formation of the metal carbides could not be achieved.